DOI: 10.1002/ejic.201001004

Local Structure in Americium and Californium Hexacyanoferrates – Comparison with Their Lanthanide Analogues

Gaelle Dupouy,[a] Isabelle Bonhoure,[a][‡] Steven D. Conradson,[b] Thomas Dumas,[a] Christoph Hennig,[c] Claire Le Naour,[d] Philippe Moisy,[a] Sébastien Petit,[a] Andreas C. Scheinost,[c] Eric Simoni,[d] and Christophe Den Auwer*[a]

Keywords: Actinides / Americium / Californium / X-ray absorption spectroscopy / EXAFS spectroscopy

Metal hexacyanoferrates are well known molecular solids for a large variety of cations, although very little has been described for actinide adducts. Two new members of actinide(III) hexacyanoferrates were synthesized with the cations americium and californium. They were structurally characterized by infrared and X-ray absorption spectroscopy. Combined EXAFS data at the iron K edge and actinide L_3 edge provide evidence for a three-dimensional model for these two new compounds. Structural data in terms of bond lengths were compared to those reported for the parent lanthanide(III) compounds, neodymium and gadolinium hexacyanoferrates, respectively: the americium compound with $KNd^{III}Fe^{II}(CN)_6{\cdot}4H_2O$ and the californium compound with $KGd^{III}Fe^{II}(CN)_6{\cdot}3.5H_2O$ and $KGd^{III}Fe^{II}(CN)_6{\cdot}3H_2O$. This comparison between actinide and lanthanide homologues has been carried out on the basis of ionic radii considerations. The americium and neodymium environments appear to be very similar and are arranged in a tricapped trigonal prism polyhedron of coordination number 9 (CN: 9), in which the americium atom is bonded to six nitrogen atoms and to three water molecules. For the californium adduct, a similar comparison and bond length and angle values derived from EXAFS studies suggest that the californium cation sits in a bicapped trigonal prism (CN: 8) as in $KGd^{III}Fe^{II}(CN)_6{\cdot}3H_2O$. This arrangement differs from that in the structure of $KGd^{III}Fe^{II}(CN)_6{\cdot}3.5H_2O$, in which the gadolinium atom is surrounded by 9 atoms. This is one of the rare pieces of information revealed by EXAFS spectroscopy for americium and californium in comparison to lanthanide atoms in molecular solid compounds. A discussion on the decrease in bond length and coordination number from americium to californium is also provided, on the basis of crystallographic results reported in the literature for actinide(III) and lanthanide(III) hydrate series.

Introduction

The molecular physical chemistry of actinides has been the subject of constant interest. Fuel reprocessing from nuclear power plants, repository risk assessment, potential toxicological impact of spent nuclear fuel, and nonproliferation of nuclear weapons are some of the major issues in countries using nuclear energy. For example, nuclear fuel reprocessing based on hydrometallurgical techniques is one of the motivations behind both fundamental and applied research in actinide chemistry. The concept of ligand selectivity and/or affinity finds applications in liquid/liquid separation processes, design of sequestering agents, etc. From that perspective, donor ligands have always been of interest as potential candidates for the liquid/liquid extraction processes.[1] From a fundamental aspect, the molecular chemistry of actinides is still a challenging issue for physical chemists, because the understanding of the properties of heavy cations is still hampered by their large number of electrons. As a consequence, a better understanding of bonding (structure and properties) in actinide molecules has been the subject of considerable effort from the community. In comparison to transition metal chemistry, very little has been understood about the structural and electronic properties of actinide molecules. An additional and essential point of debate comes from the comparison with the parent lanthanide family with a large number of electrons but very different electronic properties. This important topic finds also important industrial applications in nuclear fuel reprocessing and subsequent lanthanide or minor actinide separation. From a structural point of view, transplutonium chemistry and lanthanide chemistry are often believed to yield similar molecular edifices, although very few points of comparison have been reported because of the difficulty to work with weighable amounts of elements beyond curium.

Among the quasi-infinity of synthetic molecular edifices, the hexacyanometallate family is well known in transition

[a] CEA, Nuclear Energy Division, RadioChemistry and Processes Department,
30207 Bagnols sur Cèze, France
E-mail: christophe.denauwer@cea.fr
[b] Los Alamos National Laboratory, Material Science and Technology Division,
Los Alamos, NM 87545, USA
[c] Forschungszentrum Dresden-Rossendorf,
01314 Dresden, Germany
[d] University Paris XI Orsay, IPN Orsay,
91405 Orsay, France
[‡] Now an independent fellow in Barcelona, Spain

metal chemistry to behave with remarkable electronic properties. It is also an interesting example of building block chemistry with structurally defined subfamilies. By controlling the structure, electronic delocalization may be tuned up or down in order to design systems that exhibit a large variety of physical properties. For instance, several molecular three-dimensional Fe/Co analogues of Prussian blue can exhibit both thermally induced and photoinduced reversible electron transfer.[2] The recent publication of Hocking et al. underlines the well-known particularity of the iron–cyano bond in ferri- and ferrocyanide.[3] A considerable number of studies have also been devoted to the structural and electronic characterization of Prussian blue derivatives. Indeed, for a summary the reader can consult the review of Ohba et al.[4] For the f elements, lanthanide hexacyanometallate derivatives have also been reported; however, they present little interest as electron delocalized edifices, because of the localized properties of the 4f electrons, as mentioned above in the Introduction. Still, a neodymium hexacyanoferrate compound, $[Nd(DMF)_4(H_2O)_3Fe(CN)_6]\cdot H_2O$, has been shown to exhibit photomagnetic switching.[5]

In the field of nuclear chemistry, and more precisely lanthanide–actinide separation, some properties of lanthanide hexacyanoferrates have been described and compared to those of compounds with the parent element americium.[6]

From a structural point of view, the $KLn^{III}/Fe^{II}(CN)_6\cdot xH_2O$ (Ln: lanthanide atom) family can be divided into three series. The first one, with Ln = La to Nd, presents the general formula $KLnFe^{II}(CN)_6\cdot 4H_2O$.[7,8–11] These compounds crystallize in the hexagonal $P6_3/m$ space group. The second series has a unique representative, $KSmFe^{II}(CN)_6\cdot 3H_2O$, which crystallizes in a monoclinic group ($P2_1/m$).[12] For these two series, the nine-coordinate lanthanide cation is bound to six $\{Fe(CN)_6\}$ motifs and to three water molecules in a distorted trigonal tricapped prism. Finally, the third series involves Ln = Eu to Lu. They all occur in the orthorhombic space group: $KLnFe^{II}(CN)_6\cdot 3.5H_2O$ crystallizes in the *Cmcm* space group,[13,14,15] while $KLnFe^{II}(CN)_6\cdot 3H_2O$ crystallizes in the *Pnma* (or *Pbnm*, with $\{a,b,c\} = \{c,a,b\}$) space group.[16,17] The difference between the two space groups is the coordination number of the lanthanide atom: in the *Cmcm* group the lanthanide cation is nine-coordinate as in the La–Nd series; in the *Pnma* group the lanthanide cation is eight-coordinate to six nitrogen atoms and only two water molecules. In the nine-coordinate lanthanide compounds, the $LnN_6(H_2O)_3$ polyhedron forms a tricapped trigonal prism in which the lanthanide is bonded to six nitrogen atoms in prismatic sites and three water molecules in the capping positions. In the eight-coordinate lanthanide compounds, the $LnN_6(H_2O)_2$ polyhedron forms a square antiprism or a bicapped trigonal prism.

For the $Ln^{III}/Fe^{III}(CN)_6\cdot xH_2O$ family, only two series occur. The first one, with general formula $LnFe^{III}(CN)_6\cdot 5H_2O$, contains Ln = La to Nd and is isostructural with the first ferrocyanide series (one water molecule replaces one potassium atom).[18–20] The second series contains Ln = Pr to Lu with general formula $LnFe^{III}(CN)_6\cdot 4H_2O$.[21–23] It crystallizes in the *Cmcm* space group, but the coordination number of the lanthanide atom is different from that in the $KLnFe^{II}(CN)_6\cdot 3.5H_2O$ series: it is eight-coordinate and the $LnN_6(H_2O)_2$ polyhedron forms a square antiprism. As a result, both praseodymium and neodymium hexacyanoferrate complexes can crystallize in the $P6_3/m$ (with five water molecules) or in the *Cmcm* (with four water molecules) space groups. However, they have been shown to be more stable in the *Cmcm* space group by loss of a water molecule.

For the actinide family, the first mention of plutonium hexacyanoferrate was made in the 1950s during the Manhattan project.[24] Since then, a variety of $M_x(UO_2)_y[Fe(CN)_6]_z\cdot wH_2O$ compounds have been synthesized and used as sorbents,[25] but only the uranyl adduct of these actinide hexacyanoferrate complexes has been structurally characterized.[26] The X-ray powder diffraction of complex $Th^{IV}[Fe^{II}(CN)_6]\cdot 5H_2O$ has also been reported: it crystallizes in the hexagonal space group as $KLn^{III}KFe^{II}(CN)_6\cdot 4H_2O$ does.[27]

A few years ago we started describing the molecular structure of the materials formed by $\{Fe(CN)_6\}$ building blocks and actinide(IV) atoms (An = Th, U, Np).[28] Particular interest was to describe the distinct nature of the An–NC–Fe (An = actinide cation) bond, keeping in mind that the cyano ligand is one of the preferred candidates to foster electronic delocalization. Another aspect that attracted interest was the structural consequences of incorporating rigid building blocks in the large and often flexible actinide coordination sphere. It was also found from combined X-ray absorption spectroscopy (XAS) and X-ray diffraction studies that actinide(IV) compounds were isostructural to the earlier $KLn^{III}KFe^{II}(CN)_6\cdot 4H_2O$ compounds (hexagonal) in contrast with the cubic phases usually observed for transition metals. In all cases, the EXAFS data indicate that the hexacyanoferrate molecular entity is conserved as a rigid block, and the lanthanide or actinide cation is incorporated through nitrogen bonding of the cyano ligands. The remainder of the coordination sphere of the cation is filled with water molecules.

In this paper, we explore the structural comparison between An^{III} and Ln^{III} for two actinide elements, americium and californium. They are both located after the turning point within the actinide series, when oxidation +3 becomes predominant as in the lanthanide family. Americium is considered as the first element of the series with stronger lanthanide character (it is often considered as a turning point in actinide chemical properties), and californium is the heaviest element available in the laboratory for weighable chemistry. Both elements are also very good representatives of +3 actinide chemistry, no other stable oxidation state being achievable under our experimental conditions. From an electronic point of view, the second half of the actinide series is considered to bear relatively more localized 5f character, as observed through the entire lanthanide series for 4f electrons. From the structural point of view addressed in this article, the comparison between the lanthanide on the one hand and americium/californium adducts on the other hand raises the question of the influence of actinide con-

tractions on coordination modes (polyhedron, coordination number). This is particularly interesting in the case exposed here when semirigid building blocks are used to form the extended structure. In order to characterize the americium and californium coordination spheres, we report here a combination of extended X-ray absorption fine structure (EXAFS) and IR spectroscopic data.

Results

Infrared Spectroscopy

The IR spectra of $Am^{III}/Fe^{II}(CN)_6$ (denoted **Am^{III}/Fe^{II}** in the following discussion) and $Cf^{III}/Fe^{II}(CN)_6$ (**Cf^{III}/Fe^{II}**) were recorded between 4000 and 650 cm^{-1} and compared to the spectra of **Nd^{III}/Fe^{II}** and **Nd^{III}/Fe^{III}** respectively. All spectra exhibit the absorption band corresponding to the O–H stretch around 3600 cm^{-1} and absorption bands of the H–O–H bending mode around 1600 cm^{-1} (not shown), which confirms the presence of coordinated water molecules in the compounds. Absorption bands with a pronounced shoulder near 3350 cm^{-1} can be attributed to hydroxy stretching bands characteristic of zeolite water.[13] The main bands due to the cyano stretching vibration are located between 2000 and 2200 cm^{-1} and are shown in Figure 1. The spectra of the starting materials $K_3[Fe^{III}(CN)_6]$ (denoted **$/Fe^{III}$**) and $K_4[Fe^{II}(CN)_6]\cdot 3H_2O$ (denoted **$/Fe^{II}$**) are also reported in Figure 1. The spectrum of the $[Fe^{III}(CN)_6]^{3-}$ motif exhibits a peak at 2116 cm^{-1}, which represents the signature of the cyano groups of **$/Fe^{III}$** units that are slightly coordinated with potassium atoms.[29] The spectrum of the $[Fe^{II}(CN)_6]^{4-}$ motif exhibits two bands at 2022 and 2039 cm^{-1}. They are attributed to the cyano stretching vibration of the ligands that are slightly coordinated with potassium atoms. The presence of two peaks can be explained by the fact that $K_4[Fe^{II}(CN)_6]\cdot 3H_2O$ can crystallize in two crystallographic structures with a slight difference in CN bond lengths.[30] The spectrum of **Am^{III}/Fe^{II}** exhibits a band at 2069 cm^{-1}. In comparison with **$/Fe^{II}$**, the peak position is shifted to higher energies. This suggests that coordination of the cyano groups of the $\{Fe(CN)_6\}$ motif occurs, as in the $KLn^{III}Fe^{II}(CN)_6\cdot xH_2O$ series. On the other hand, the value of 2069 cm^{-1} compares very well with that of the cyano band of the **Nd^{III}/Fe^{II}** compound, shown in Figure 1 at 2056 cm^{-1} and also reported by Milligan et al.[10] The spectrum of **Cf^{III}/Fe^{II}** exhibits a larger band at 2083 cm^{-1} (with a lower wavenumber shoulder, not explained), this value being also in the expected spectral range of M^{III}/Fe^{II} compounds. These values are comparable but rank in the order 2056 cm^{-1} (for Nd) $<$ 2069 cm^{-1} (for Am) $<$ 2083 cm^{-1} (for Cf). This slight increase in wavenumber from Nd to Cf may be simply explained in a first approximation by an increase of the bond force constant from Nd to Am because of the increase in mass and from Am to Cf because of the decrease in bond length, everything else (the Fe–CN fragment) being identical. The value reported by Goubard et al. for $KGd^{III}Fe^{II}(CN)_6 3\cdot 5H_2O$[14] (2076 cm^{-1}) also agrees very well with these numbers.[14]

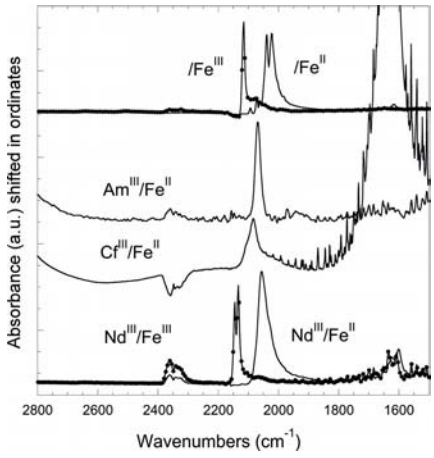

Figure 1. Infrared spectra showing the cyano stretching vibration bands (between 1700 and 2400 cm^{-1}) of $K_4Fe^{II}(CN)_6\cdot 3H_2O$, $K_3Fe^{III}(CN)_6$, **Am^{III}/Fe^{II}**, and **Cf^{III}/Fe^{II}**. Comparison with **Nd^{III}/Fe^{II}** $[KNd^{III}Fe^{II}(CN)_6\cdot nH_2O]$ and **Nd^{III}/Fe^{III}** $[Nd^{III}Fe^{III}(CN)_6\cdot nH_2O]$.

XANES, EXAFS Studies

Figure 2 shows the experimental XANES spectrum at the Cf and Am L_3 edges of **Am^{III}/Fe^{II}** and **Cf^{III}/Fe^{II}** and the Fe K edge of **Am^{III}/Fe^{II}**. The absorption edges have all been rescaled in energy with respect to the edge ramp for comparison. As expected, the Am and Cf L_3 edges are very similar, since both cations are at the same oxidation state in similar environments. The Fe K edge of **Am^{III}/Fe^{II}** exhibits the characteristic sharp white line and an intense first oscillation, which is a characteristic of the $\{Fe(CN)_6\}$ unit.[28] From a descriptive point of view, the absence of any intense pre-edge also confirms the octahedral environment of iron.

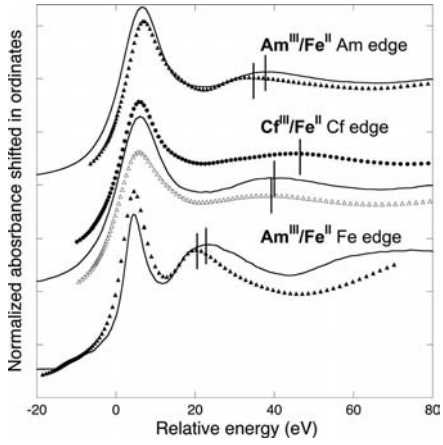

Figure 2. Experimental XANES spectra at the Am L_3 edge and Fe K edge of **Am^{III}/Fe^{II}** and at the Cf L_3 edge of **Cf^{III}/Fe^{II}** (solid line). Comparison with the simulated spectra (Feff84) of $KNd^{III}Fe^{II}(CN)_6\cdot 4H_2O$[10] (filled triangles), $KGd^{III}Fe^{II}(CN)_6\cdot 3H_2O$[17] (hollow triangles) and $KGd^{III}Fe^{II}(CN)_6\cdot 3.5H_2O$[14] (filled circles). All spectra have been shifted in energy with respect to the absorption ramp.

The actinide cation environments in **Am^{III}/Fe^{II}** and **Cf^{III}/Fe^{II}** were further characterized by EXAFS spectroscopy at the actinide L_3 edge and at the iron K edge for **Am^{III}/Fe^{II}**.

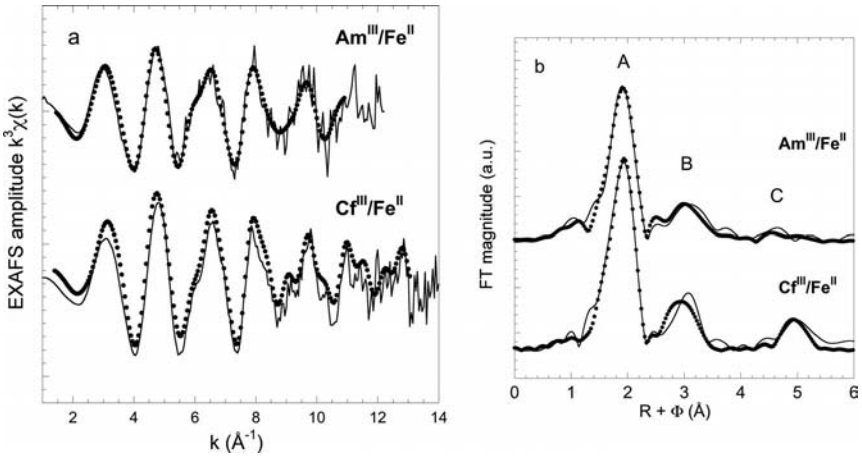

Figure 3. (a) Experimental (solid line) and adjusted (circles) EXAFS oscillations at the An L_3 edge of **Am^{III}/Fe^{II}** and **Cf/Fe^{II}**. (b) Corresponding experimental (solid line) and adjusted (circles) moduli of the Fourier transform of the EXAFS spectra.

At the actinide L_3 edge, the EXAFS spectra of **Am^{III}/Fe^{II}** and **Cf^{III}/Fe^{II}** and the corresponding modulus part of the Fourier transform are represented in Figure 3a,b. A qualitative comparison of the spectra shows that they present three analogous peaks (A, B, and C), which may be attributed to coordination of the actinide cation with the $\{Fe(CN)_6\}$ building blocks (N, C, and Fe, respectively), as observed for model compound **Lu^{III}/Fe^{III}/DMF** and described in detail in the Experimental Section. For **Am^{III}/Fe^{II}**, the weakness of peak C may account for a more highly disordered contribution than that for **Cf^{III}/Fe^{II}**. This may qualitatively be explained by the experimental conditions: the XAS spectrum of **Am^{III}/Fe^{II}** was recorded about 20 d after synthesis (time for sample transportation to SSRL), while the spectrum of **Cf^{III}/Fe^{II}** was recorded at ESRF only few days after synthesis. Although the absence of significant chemical evolution in time has been verified by parallel IR spectroscopy, amorphization due to actinide-specific activity (1.26×10^6Bq/g for ^{241}Am, 1.51×10^6Bq/g for ^{249}Cf) is certainly not excluded. Given the difference in sample transportation delay, **Am^{III}/Fe^{II}** is probably more disordered than **Cf^{III}/Fe^{II}**, and this phenomenon is particularly sensitive in the long-range order. The EXAFS spectrum of **Am^{III}/Fe^{II}** at the iron K edge and the corresponding modulus part of the Fourier transform are represented in Figure 4a,b. As expected it exhibits two majors peaks, D and E, as in model compound **Lu^{III}/Fe^{III}/DMF**, indicating that the $\{Fe(CN)_6\}$ motif is preserved. It also qualitatively corroborates the observation at the actinide L_3 edge and leads to the conclusion that the cyano ligand bridges the iron and actinide cations. Considering this observation and the validation of our fitting procedure for **Lu^{III}/Fe^{III}/DMF**, both iron K and americium L_3 edges of **Am^{III}/Fe^{II}** have been adjusted together with the set of linked parameters described in the Experimental Section. The two-edge fit methodology based on a combination of cross-linked parameters allows to obtain metrical data along the An–NC–Fe chain with satisfying accuracy. On the modulus part of the FT (Figures 3b and 4b), peaks A, B, C, D, and E are reproduced with a very good agreement as reported by the fit parameters in Table 1. Values of the Debye–Waller factors are comparable for the first shell but differ significantly for further shells

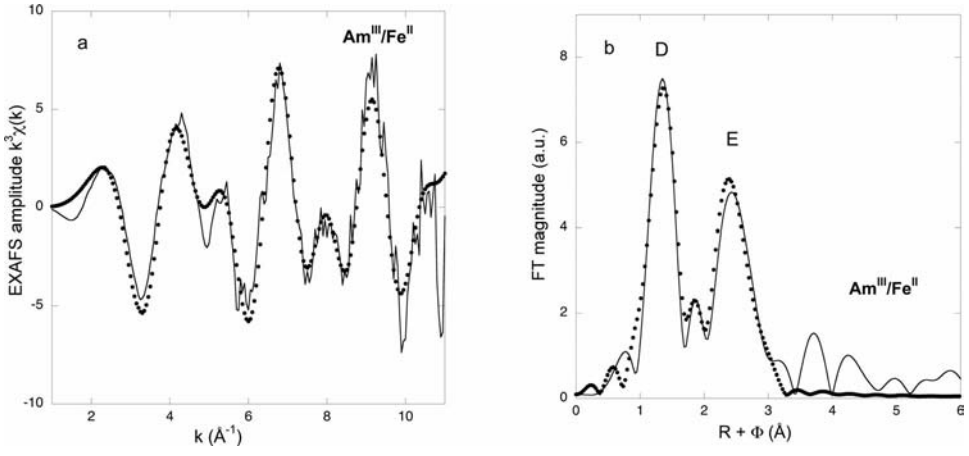

Figure 4. (a) Experimental (solid line) and adjusted (circles) EXAFS oscillations at the Fe K edge of **Am^{III}/Fe^{II}**. (b) Corresponding experimental (solid line) and adjusted (circles) moduli of the Fourier transform of the EXAFS spectra.

(the coordination numbers being fixed by the model used), as these materials are expected to be significantly disordered (radiation from the actinide-specific activity might be an additional origin of increased disorder as mentioned above).

Table 1. Best-fit EXAFS parameters for **Am^{III}/Fe^{II}** and **Cf^{III}/Fe^{II}**. σ^2 is the Debye–Waller factor, S_0^2 is the global amplitude factor, Δe_0 is the energy shift parameter in eV, R is the quality factor of the fit in R space, and ε is the average noise of the spectrum in $k^3\chi(k)$. Numbers in italics have been linked or fixed. Uncertainties are in round brackets.

Am^{III}/Fe^{II}	**Cf^{III}/Fe^{II}**	S_0^2, Δe_0, ε, R
Fe K edge		
6 C at 1.88(1) Å	*6* C at *1.88(1)* Å	
σ^2 = 0.0025 Å^2	σ^2 = *0.0025* Å^2	0.7, 0.22 eV
6 N at 3.00(1) Å	*6* N at *3.00(1)* Å	0.004, 4.0%
σ^2 = 0.0019 Å^2	σ^2 = *0.0019* Å^2	
Am L_3 edge	Cf L_3 edge	
6 N at 2.49(1) Å	*6* N at 2.44(1) Å	**Am^{III}/Fe^{II}**
σ^2 = 0.0060 Å^2	σ^2 = 0.0068 Å^2	1.1, 6.9 eV
3 O at 2.69(3) Å	*2* O at 2.54(1) Å	0.003, 3.1%
σ^2 = 0.0109 Å^2	σ^2 = 0.0120 Å^2	
6 C at 3.52(1) Å	*6* C at 3.51(1) Å	
σ^2 = 0.0020 Å^2	σ^2 = 0.0090 Å^2	**Cf^{III}/Fe^{II}**
6 Fe at 5.33(2) Å	*6* Fe at 5.35(2) Å	1.1, 4.9 eV
σ^2 = 0.0140 Å^2	σ^2 = 0.0050 Å^2	0.002, 2.7%
θ = 152(10)°	θ = 159(10)°	

For **Cf^{III}/Fe^{II}** the absence of the iron K edge spectrum makes it impossible to use the same procedure of geometrical parameterization in the EXAFS data fitting. To overcome this difficulty, we considered the {$Fe(CN)_6$} motif as invariant from Am to Cf. In order to validate this approximation, we carried out a survey of the available crystal structures of $KLn^{III}Fe^{II}(CN)_6{\cdot}xH_2O$ (refs.[7–17]). In all of these structures, the distances within the iron octahedron are on the average d(FeC) = 1.91 ± 0.02 Å and d(CN) = 1.15 ± 0.01 Å. The fluctuations for both distances are in the order of the EXAFS fitting uncertainties. Therefore, from the EXAFS point of view, the {$Fe(CN)_6$} motif may be considered as a rigid block in the above-mentioned series. Consequently, we considered that the {$Fe(CN)_6$} motif is similar for **Am^{III}/Fe^{II}** and **Cf^{III}/Fe^{II}**. This is also corroborated by the fact that Am^{III} and Cf^{III} are cations of similar properties with positions Z to Z + 3 in the periodic table. Furthermore, we recall that the assumption of considering a rigid {$Fe(CN)_6$} motif does not lock the bond angle and distances on the An–N,O side of the structure in the fit. Accordingly, the iron K edge of **Am^{III}/Fe^{II}** has been injected in the fitting procedure of **Cf^{III}/Fe^{II}** (numbers in italics in Table 1). The corresponding best fit parameters at the californium edge are presented in Table 1. As for **Am^{III}/Fe^{II}**, in the modulus part of the FT at the actinide edge (Figure 3b), peaks A, B, and C are reproduced with a very satisfactory agreement.

For comparison, a fit of the single shells (after back Fourier filtering) was carried out with free distance parameters (coordination numbers being kept constant). For **Am^{III}/Fe^{II}**: *6* N at 2.50 Å (σ^2 = 0.0071 Å^2) and *3* N at 2.73 Å (σ^2 = 0.0181 Å^2), *6* Fe at 5.35 Å (σ^2 = 0.0180 Å^2); for **Cf^{III}/Fe^{II}**: *6* N at 2.45 Å (σ^2 = 0.0074 Å^2) and *3* N at 2.50 Å (σ^2 = 0.0158 Å^2), *6* Fe at 5.32 Å (σ^2 = 0.0092 Å^2); around Fe in **Am^{III}/Fe^{II}**: *6* C at 1.87 Å (σ^2 = 0.0029 Å^2) (all fits with R factors less than 0.5% except for the Fe contribution in **Am^{III}/Fe^{II}** and **Cf^{III}/Fe^{II}**, where amplitude discrepancies increased the R factor to 10%, partly because only one single scattering contribution was considered). The data obtained with the parameterized adjustment and the above single-shell model agree very satisfactorily within 0.02–0.03 Å (see Table 1 for comparison).

A comparison of the metric parameters obtained for **Am^{III}/Fe^{II}** and **Cf^{III}/Fe^{II}** shows that they all are comparable but not similar: going towards californium brings a net decrease in all distances around the actinide cation, in agreement with the actinide contraction: Δd(AnN) = –0.05 Å and Δd(AnO) = –0.15 Å from Am to Cf. This trend may also explain the increase in the cyano stretching frequency described above in the IR spectra. The bond angle θ between An–N and N≡C–Fe is also always inferior to 180°, as expected from the comparison with all the lanthanide analogues.

Finally, Figure 2 compares the experimental XANES spectra of **Am^{III}/Fe^{II}** at the Am L_3 and Fe K edges and of **Cf^{III}/Fe^{II}** at the Cf L_3 edge to simulations carried out from the lanthanide analogues: $KNd^{III}Fe^{II}(CN)_6{\cdot}3H_2O$ for the Am L_3 and Fe K edges; $KGd^{III}Fe^{II}(CN)_6{\cdot}3H_2O$ and $KGd^{III}Fe^{II}(CN)_6{\cdot}3.5H_2O$ for the Cf L_3 edge. Simulations were performed here by replacement of the lanthanide atomic number in the input file by the corresponding actinide number (i.e. Nd replaced by Am, Gd replaced by Cf), everything else being kept equal to the crystal structures (see Experimental Section for details). Although the direct comparison must be taken with care, it appears clearly that in the case of **Cf^{III}/Fe^{II}**, the position of the first oscillation (vertical mark in Figure 2) is in better agreement with that of simulated $KCf(Gd)^{III}Fe^{II}(CN)_6{\cdot}3H_2O$ than with that of simulated $KCf(Gd)^{III}Fe^{II}(CN)_6{\cdot}3.5H_2O$. In the case of **$Am^{III}/Fe^{II}$**, at both the Fe and Am edges, although the agreement is not perfect, the experimental and simulated spectra of $KAm(Nd)^{III}Fe^{II}(CN)_6{\cdot}3H_2O$ compare satisfactorily. Keeping the same simulation parameters, the EXAFS spectra of $KGd(Cf)^{III}Fe^{II}(CN)_6{\cdot}3H_2O$ and $KGd(Cf)^{III}Fe^{II}(CN)_6{\cdot}3.5H_2O$ were also simulated from the crystallographic structure of both gadolinium compounds (again replacing Gd by Cf in the simulation). Figure 5 shows the EXAFS spectra of the two simulations compared to the experimental EXAFS spectrum of **Cf^{III}/Fe^{II}**. In the figure, the e_0 value of the experimental spectrum has been adjusted in order for all the spectra to be compared. Without adjustment of any of the distances in the simulation, the similarity between the EXAFS spectra of $KGd(Cf)^{III}Fe^{II}(CN)_6{\cdot}3H_2O$ and **Cf^{III}/Fe^{II}** is remarkable. On the contrary, strong differences in the beating modes occur after 6 Å^{-1} between the oscillations of $KGd(Cf)^{III}Fe^{II}(CN)_6{\cdot}3.5H_2O$ and of **Cf^{III}/Fe^{II}**. This observation strongly confirms all of the above assumptions that **Cf^{III}/Fe^{II}** is similar to $KGd^{III}Fe^{II}(CN)_6{\cdot}3H_2O$.

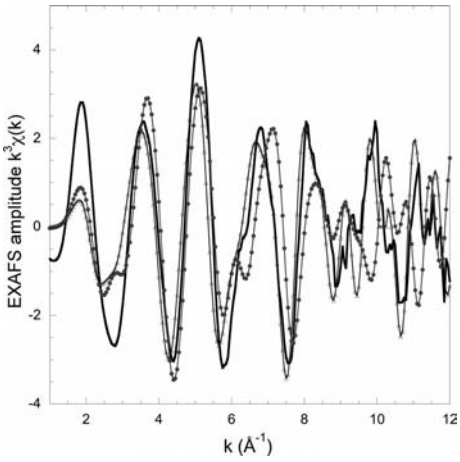

Figure 5. Experimental EXAFS spectrum at the Cf L_3 edge of **Cf^{III}/Fe^{II}** (solid line). Comparison with the simulated spectra (Feff84) of $KGd^{III}Fe^{II}(CN)_6{\cdot}3H_2O$[17] (triangles) and $KGd^{III}Fe^{II}(CN)_6{\cdot}3.5H_2O$[14] (circles).

Discussion

This work aims to tackle the structure of two representatives of the actinide(III) hexacyanoferrate family, namely **Am^{III}/Fe^{II}** and **Cf^{III}/Fe^{II}**, and compare the actinide coordination polyhedra with those of the lanthanide equivalents. The important question to be addressed in this comparison is how do the actinide(III) polyhedra evolve as the atomic number increases, especially in the case of semirigid building block chemistry, and how does this evolution compare with those of the lanthanide equivalents? Because of the similarity between the lanthanide +III and transplutonium +III chemistry, we start this discussion with a direct comparison of the two families on the basis of ionic radii considerations. At CN: 8, the Am^{3+} ionic radius is similar to that of Nd^{3+} (r_{Nd} = 1.109 Å, r_{Am} = 1.09 Å, CN: 8) and at CN: 6, the Cf^{3+} ionic radius is between that of Eu^{3+} and that of Gd^{3+} (r_{Eu} = 0.947 Å, r_{Cf} = 0.945 Å, r_{Gd} = 0.938 Å, CN: 6).[31,32] Within this framework, **Am^{III}/Fe^{II}** may be compared to $Nd^{III}Fe^{II}(CN)_6{\cdot}xH_2O$. In the Introduction, we have explained that $KLn^{III}Fe^{II}(CN)_6{\cdot}xH_2O$ (Ln = Eu to Lu) exhibits two possible crystalline forms that have been reported for solely Ln = Gd. Table 2 presents a summary of the **Am^{III}/Fe^{II}** and **Cf^{III}/Fe^{II}** bond lengths obtained from Table 1 and compares them to those of the neodymium and gadolinium analogues. One shall keep in mind, however, the assumption in EXAFS fitting that all the $\{Fe(CN)_6\}$ motifs were kept identical to that in **Am^{III}/Fe^{II}**. A more detailed investigation of the bond lengths around the neodymium cations indicates that in $Nd^{III}Fe^{III}(CN)_6{\cdot}xH_2O$ [and more generally in the $Ln^{III}Fe^{III}(CN)_6{\cdot}xH_2O$ family], d(LnN) is always greater than d(LnO), whereas in $KNd^{III}Fe^{II}(CN)_6{\cdot}xH_2O$ [the $KLn^{III}Fe^{II}(CN)_6{\cdot}xH_2O$ family] it is the opposite.

In the following discussion we detail the comparison of **Am^{III}/Fe^{II}** with the neodymium equivalent on the one hand, and **Cf^{III}/Fe^{II}** with the gadolinium equivalents on the other hand. In $KNd^{III}Fe^{II}(CN)_6{\cdot}4H_2O$, the neodymium cation is ninefold coordinated to six nitrogen atoms [d(NdN) = 2.52 Å] and three water molecules [d(NdO) = 2.68 Å]. A direct comparison between the distances obtained by EXAFS for **Am^{III}/Fe^{II}** and the values above suggests that the americium and neodymium environments are analogous. Therefore, by analogy, **Am^{III}/Fe^{II}** must contain ninecoordinate $\{AmN_6(H_2O)_3\}$ units. Consequently, the americium polyhedron may be attributed to a tricapped trigonal prism in which the americium is bonded to six nitrogen atoms in apical sites and to three water molecules in the equatorial plane. Although the distances within the $\{Fe(CN)_6\}$ blocks are slightly shorter in the americium compound than in the neodymium one, this difference lies within the range mentioned above in the survey of lanthanide compounds (–0.02 Å).

Comparison between the ionic radii of californium and gadolinium suggests that **Cf^{III}/Fe^{II}** may crystallize as $KGd^{III}Fe^{II}(CN)_6{\cdot}3.5H_2O$[14] or as $KGd^{III}Fe^{II}(CN)_6{\cdot}3H_2O$.[17] As described in the introduction of this paper, gadolinium adducts may occur in two different forms: $KGd^{III}Fe^{II}(CN)_6{\cdot}3.5H_2O$ crystallizes in orthorhombic space group *Cmcm* with a coordination number of nine, while $KGd^{III}Fe^{II}(CN)_6{\cdot}3H_2O$ crystallizes in orthorhombic space group *Pnma* with a coordination number of eight. As shown in Table 2, the values of d(GdN), d(GdO), and θ are 2.35 Å, 2.50 Å, and 171.2° for $KGd^{III}Fe^{II}(CN)_6{\cdot}3.5H_2O$ and 2.43 Å, 2.57 Å, and 162.1° for $KGd^{III}Fe^{II}(CN)_6{\cdot}3H_2O$, respectively. In comparison, the metrical parameters for **Cf^{III}/Fe^{II}** are 2.44 and 2.54 Å (again keeping in mind that the $\{Fe(CN)_6\}$ motif has been "imported" from **Am^{III}/Fe^{II}**). Matching the bond length between californium and gadolinium suggests **Cf^{III}/Fe^{II}** to be equivalent to $KGd^{III}Fe^{II}(CN)_6{\cdot}3H_2O$ (corresponding to the *Pnma* space group) and not to $KGd^{III}Fe^{II}(CN)_6{\cdot}3.5H_2O$ (corresponding to the *Cmcm* space group). Consequently, by analogy with $KGd^{III}Fe^{II}(CN)_6{\cdot}3H_2O$, the californium cation must sit in an eightfold coordinated polyhedron, $\{CfN_6(H_2O)_2\}$, in contrast to the ninefold coordinated polyhedron for the americ-

Table 2. Bond lengths and angles reported in Table 1 for **Am^{III}/Fe^{II}** and **Cf^{III}/Fe^{II}** (EXAFS) compared to the literature data (X-ray diffraction data) for the neodymium and gadolinium analogues.

Distances [Å]	An–O	An–N	N–C	C–Fe	An–Fe	θ [°]
Am^{III}/Fe^{II}	2.69(3)	2.49(1)	1.12(1)	1.88(1)	5.33(2)	152(10)
$KNd^{III}Fe^{II}(CN)_6{\cdot}4H_2O$[10]	2.685(3)	2.518(3)	1.166(4)	1.903(3)	5.469(3)	156.7(5)
Cf^{III}/Fe^{II}	2.54(1)	2.44(1)	1.12(1)	1.88(1)	5.35(2)	159(10)
$KGd^{III}Fe^{II}(CN)_6{\cdot}3.5H_2O$[14]	2.50(1)	2.35(1)	1.16(1)	1.92(1)	5.34(1)	171.2(4)
$KGd^{III}Fe^{II}(CN)_6{\cdot}3H_2O$[17]	2.570(4)	2.431(5)	1.163(7)	1.905(5)	5.32(1)	162.1(4)

ium adduct. In this gadolinium structure, the polyhedron is best described as a bicapped trigonal prism. Qualitatively, the cyano stretching frequency in the order Nd < Am < Cf is in agreement with the relative decrease in M–N distances in the order Nd ≈ Am > Cf. One shall note that, although the bond angles θ obtained from the fit of **Am^{III}/Fe^{II}** and **Cf^{III}/Fe^{II}** agree with the above assumption, these values must be taken with particular care, given the high uncertainty related to them.

The striking point in this comparison is the decrease in coordination number by one unit upon going from neodymium (americium) to gadolinium (californium), from trigonal tricapped prism to trigonal bicapped prism. As explained in the Introduction, in the $KLn^{III}/Fe^{II}(CN)_6{\cdot}xH_2O$ series, two different lanthanide coordination polyhedra occur. For Ln = La to Sm, a nine-coordinate configuration with three coordinated water molecules is observed. According to the EXAFS results, **Am^{III}/Fe^{II}** fits in this category. For the end of the lanthanide series, Ln = Eu to Lu, there are two different crystallographic structures, which involve two different coordination spheres: the *Cmcm* space group with a similar nine-coordinate coordination sphere as for the beginning of the series or the *Pnma* space group with an eight-coordinate coordination sphere. In the latest case, a coordinated water molecule is ejected from the equatorial plane, which results in space group switch. This reduction of coordination number for the end of the lanthanide series accounts for contraction of the cation size, which results in the loss of one water molecule. According to EXAFS data, **Cf^{III}/Fe^{II}** falls into this family by analogy with the gadolinium analogue.

Additional points of comparison can be found in between the lanthanide(III) and heavy actinide(III) coordination spheres in hydrates. Taking advantage of the EXAFS sensitivity of local structure in disordered media, the cation environment has also been probed in the aquo systems.[33] For the actinide(III), it has been lately discussed in full detail by Skanthakumar et al. for the curium cation in the hydrate form and in aqueous solution.[34] Generally speaking, two models of coordination spheres are most likely: a square antiprism (SA, CN: 8) and a tricapped trigonal prism (TTP, CN: 6+3). It has been described that the metal coordination sphere in the hydrates is a tricapped trigonal prism for the entire Ln^{3+} series[35] and for some of the An^{3+} series (Pu to Cm).[36] Very recently, the coordination sphere of Cf^{III} has also been discussed in more detail, both in acid medium by EXAFS and molecular dynamics[37] and in the solid state for the hydrate system.[38] The structure of the hydrate confirms the stability of the TTP polyhedron throughout the series from U to Cf (Bk not reported). In solution, both CN: 8 and CN: 9 are discussed. D'Angelo et al. have also proposed that, for the lanthanide(III) series a statistical deficiency of one water molecule in a capping position of the polyhedron occurs as the atomic number increases.[39] This assumption has also been recently discussed by Duvail et al. using molecular dynamics.[40] These examples show some similarities with the hexacyanoferrate family. A summary of the distances in the americium/californium and lanthanide hexacyanoferrates is presented in Figure 6. The Ln/An–N distances exhibit comparable values for the actinide coordination sphere in the **An^{III}/Fe^{II}** compounds and in the lanthanide family. The *d*(MN) distances decrease from americium to californium and from neodymium to gadolinium. This evolution is a consequence of the actinide and lanthanide contraction upon going to the higher atomic numbers. Conversely, the situation is very different for the distances within the $\{Fe(CN)_6\}$ motif. As already discussed, the Fe–C and C–N distances in all the lanthanide samples are similar and located between 1.89 and 1.93 Å for *d*(FeC) and 1.140 and 1.165 Å for *d*(CN). These distances are independent of the lanthanide atomic number. In **Am^{III}/Fe^{II}**, the only compound for which the EXAFS spectrum of the $\{Fe(CN)_6\}$ motif has been measured, *d*(FeC) = 1.88 Å and *d*(CN) = 1.12 Å. Both values are within the classical error bar (0.02 Å), similar to that of the lanthanide series although on the lower side of the distribution. Unfortunately, there is no other point of comparison, since the EXAFS spectrum of **Cf^{III}/Fe^{II}** at the iron K edge could not be recorded.

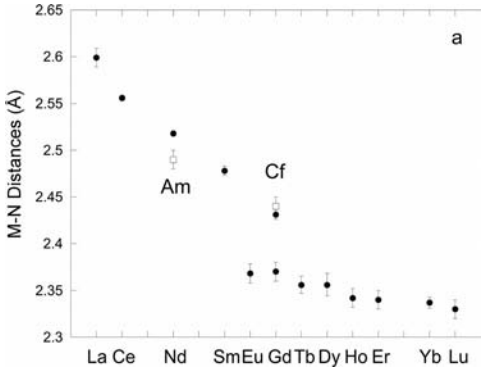

Figure 6. M–N Distances in the $KM^{III}/Fe^{II}(CN)_6{\cdot}xH_2O$ family of compounds (filled circles) from the literature[7–17] compared to those in **Am^{III}/Fe^{II}** and **Cf/Fe^{II}** (hollow squares).

Conclusions

This article describes the molecular structure of two representatives of the hexacyanoferrate family with actinide(III) cations, namely the americium and californium compounds. We have compared the structures of these new adducts to those of their homologues of the lanthanide series, namely the neodymium and gadolinium compounds. Our major interest focused on a fundamental understanding of actinide(III) chemistry, in particular in a comparison between californium chemistry and that of the parent gadolinium. Another point of interest lies in the structural consequences of incorporating rigid building blocks of the $\{M(CN)_n\}$ type in the large and often flexible actinide(III) coordination sphere in comparison to the lanthanide one. The important question in this comparison is how do the actinide(III) polyhedra evolve as atomic number increases and how does this compare with the lanthanide equivalents? This question has also been brought up for the more

flexible hydrate system. Taking advantage of the EXAFS sensitivity of local structure, both the iron and the actinide environment have been probed in a combined procedure that reduces the number of geometrical parameters.

A direct comparison between the distances obtained by EXAFS for **Am^{III}/Fe^{II}** and the reported ones for $KNd^{III}Fe^{II}(CN)_6{\cdot}4H_2O$ suggests that the americium and neodymium environment are analogous. Overall, using this analogy, the americium hexacyanoferrate(II) may be written as $KAm^{III}Fe^{II}(CN)_6{\cdot}nH_2O$. On the basis of the similarity between the ionic radii of californium and gadolinium, it is suggested that **Cf^{III}/Fe^{II}** may be compared to $KGd^{III}Fe^{II}(CN)_6{\cdot}3.5H_2O$ or to $KGd^{III}Fe^{II}(CN)_6{\cdot}3H_2O$. Matching the bond and angle values between californium and the two gadolinium compounds must be done with care. However, the observation of the metrical parameters suggests that **Cf^{III}/Fe^{II}** is closer to $KGd^{III}Fe^{II}(CN)_6{\cdot}3H_2O$ rather than $KGd^{III}Fe^{II}(CN)_6{\cdot}3.5H_2O$.

The striking point in this comparison is the decrease in coordination number by one unit upon going from neodymium (americium) to gadolinium (californium), from trigonal tricapped prism for the former compounds to trigonal bicapped prism for the latter ones. These results must be compared to the latest discussion in the literature on coordination properties of the aquo and hydrate series of Ln^{III} and An^{III}. Latest reports in the literature have involved the U–Cm, Cf series for the hydrate family. Unfortunately, additional experimental data for elements beyond curium are often lacking. This work casts light to this fundamental question by presenting data on one of the rare examples of californium molecular compounds.

Experimental Section

Materials

^{241}Americium and ^{249}Californium are radioactive materials that must be manipulated with great care in dedicated laboratories. Additional care has been taken here to reduce the dose rate by minimizing the time of manipulation and inserting lead shielding when possible.

The starting materials, $K_4Fe^{II}(CN)_6{\cdot}3H_2O$, $K_3Fe^{III}(CN)_6$, and $Lu(NO_3)_3{\cdot}xH_2O$, were commercially purchased (Aldrich or Acros). The $^{241}Am^{III}$ solution was prepared by dissolution of AmO_2 (CEA stock) in nitric acid (3 M). The solution of Am^{III} aquo was examined by gamma and alpha spectroscopy to control its purity. A part of the solution was treated with NaOH (8 M) to precipitate americium. Thus, the actinide was dissolved in HCl to obtain a solution of [Am] = 8×10^{-3} M in HCl (0.8 M). The $^{249}Cf^{III}$ solution was purified from an ill-defined old solution of ^{249}Cf (ca. 100 MBq) from IPN Orsay with a strong radiation damage to the first container. Part of the solution was concentrated to dryness, and the voluminous foamy residue was taken up in concentrated HCl. The cloudy solution was centrifuged, and the supernatant was percolated through a column filled with an anion exchanger (Bio-Rad AG-MP 1, 100–200 mesh). Then the eluted fractions were concentrated to dryness and taken up in dilute HCl. The solution obtained in this way was percolated through a column filled with a cation exchanger (Bio-Rad AG-MP 50, 100–200 mesh). The purified fractions were gathered, and the solvents were evaporated to dryness. No deposit was visible to the naked eye. The container was then rinsed with $HClO_4$ to obtain the stock californium solution. The solution of Cf^{III} aquo has been examined like the solution of Am^{III} aquo by gamma and alpha spectroscopy to control the actinide purity and concentration.

Syntheses

$[Lu^{III}(DMF)_4(H_2O)_3(Fe^{III}(CN)_6)]{\cdot}H_2O$ (Lu^{III}/Fe^{III}/DMF): The synthesis was identical to that described by Mullica.[41] After one day, yellow crystals were obtained. They were washed with acetone and dried in air.

Am^{III}/Fe^{II} Hexacyanoferrate (Am^{III}/Fe^{II}): Am^{III} (2 μmol, obtained from 250 μL of [Am] = 8×10^{-3} M solution) was mixed with a solution of $K_4Fe^{II}(CN)_6{\cdot}3H_2O$ (4 μmol) in HCl at (250 μL, 0.2 M). Upon addition of ethanol (0.5 mL), a pale blue precipitate appeared. The mixture was centrifuged and rinsed with a solution of EtOH/HCl (9:1, 0.8 M) and pure ethanol. The compound was dried in air in the glove box.

Cf^{III}/Fe^{II} Hexacyanoferrate (Cf^{III}/Fe^{II}): The synthesis is identical to that described for **Am^{III}/Fe^{II}**. Cf^{III} aquo {0. 4 μmol, obtained from 470 μL of a solution [Cf] = 8.7×10^{-4} M in $HClO_4$ (0.01 M)} was mixed with a solution of $K_4Fe^{II}(CN)_6{\cdot}3H_2O$ (1.6 μmol, 0.675 mg) in HCl (150 μL, 0.2 M). Upon addition of ethanol (1.3 mL), a pale blue precipitate appeared. The mixture was centrifuged and rinsed with pure ethanol. The compound was dried in air in the glove box.

$KNd^{III}Fe^{II}(CN)_6{\cdot}nH_2O$ and $Nd^{III}Fe^{III}(CN)_6{\cdot}nH_2O$ (Nd^{III}/Fe^{III} and Nd^{III}/Fe^{II}): The two compounds were prepared directly from neodymium nitrate (Aldrich) and ferri- or ferrocyanide in HCl (0.2 M). The precipitate was centrifuged and rinsed with pure ethanol.

IR Spectroscopy: IR spectra were recorded between 650 and 4000 cm^{-1} by using a Bruker Equinox 55 FTIR spectrometer equipped with a golden gate single-reflection ATR (Attenuated Total Reflection) system in a radioactive glove box. The ATR crystal is a 2×2 mm^2 diamond with a 0.6×0.6 mm^2 active area. The head is fitted with a flat sapphire. Powders were analyzed in the ATR cell with 4 cm^{-1} resolution and 8 scans.

X-ray Absorption Spectroscopy

Samples for XAS analysis were prepared as pellets. The powder of each compound was mixed with polyethylene in toluene and further pressed. For actinide complexes, the pellets were placed in a specific cell for radioactive materials in which the sample is doubly confined.

Spectra for **Am^{III}/Fe^{II}** were recorded at the Am L_3 edge and Fe K edge at the 11–2 beam line of SSRL (Stanford, USA). The beam line is equipped with a liquid nitrogen cooled double-crystal Si(220) monochromator, and with two collimating and focusing rhodium coated mirrors. A 30-element Ge solid-state detector was used for data collection in the fluorescence mode (Am edge) and two ionization chambers in the transmission mode (Fe edge). Energy calibration was carried out with a Zr foil (18014 eV at the absorption maximum) for the Am L_3 edge and a Fe foil (7112 eV at the first inflexion point) for the Fe K edge.

Spectra for **Cf^{III}/Fe^{II}** at the Cf L_3 edge were recorded at the Rossendorf beam line BM20 (ROBL) of ESRF (Grenoble, France). BM20 is equipped with a water-cooled double-crystal Si(111) monochromator. Higher harmonics were rejected by two collimating Pt-coated mirrors. A 13-element Ge solid-state detector was used for data collection in the fluorescence mode (Cf edge). Energy calibration was carried out with a Zr foil (18014 eV at the absorption maximum) for the Cf L_3 edge.

Spectra for **Lu^{III}/Fe^{III}/DMF** at the Lu L_3 and Fe K edges were recorded at the SAMBA beam line of SOLEIL (Saint Aubin, France). The beam line is equipped with a liquid nitrogen cooled double-crystal Si(111) monochromator, and two collimating and focusing rhodium-coated mirrors. Ionization chambers in transmission mode were used for detection. Energy calibration was carried out with an Fe foil (7112 eV at the absorption maximum).

Data treatment was carried out with the Athena code.[42] The e_0 energy was set at the maximum of the absorption edge. The EXAFS signal was extracted by subtracting a linear pre-edge background and a combination of cubic spline functions for atomic absorption background and normalized by the Lengeler–Eisenberg procedure. Pseudo-radial distribution functions (PRDF) were obtained by Fourier transformation in $k^3\chi(k)$ by using the ARTEMIS code[42] between 1.5 and 11 $Å^{-1}$. Spectral noise was calculated with the CHEROKEE[43] code after inverse Fourier transformation above 6 Å. Phases and amplitudes were calculated with the Feff82 code[44] based on the crystal structure of **Lu^{III}/Fe^{III}/DMF**, which was synthesized as a monocrystal identical to that reported in the literature.[41] In this complex, the lutetium atom is eight-coordinate to four DMF groups, three water molecules, and only one ferricyanide motif. It contains one "Fe–C–N–Lu" link, which is therefore of very weak intensity. In order to test our fitting procedure, both the iron K edge and the Lu L_3 edge of **Lu^{III}/Fe^{III}/DMF** were adjusted by using a parameterization of the metrical parameters at both edges. In the crystal structure of **Lu^{III}/Fe^{III}/DMF**, the Fe–C–N angle is equal to 177° and can be considered nearly linear, while the Lu–N–C angle (denoted as θ) is equal to 164°. In the fitting procedure, in order to decrease the number of free structural parameters, the following distances were linked: d(FeN) = d(FeC) + d(CN), $d(LuC)^2 = d(LuN)^2 + d(CN)^2 - 2d(LuN)d(CN)\cos\theta$, which lead to $d(LuFe)^2 = d(LuN)^2 + [d(CN) + d(FeC)]^2 - 2d(LuN)[d(CN) + d(FeC)]\cos\theta$. At the Fe K edge (Figure 7), the two peaks, D and E, indicate coordination between the iron atom and the cyano ligands. The first peak, D, represents the single scattering of the first shell (C atoms) and depends on the d(FeC) bond length. The second peak, E, is a combination of the single scattering of the second shell (N atoms) and of the multiple scattering of the Fe–C–N chain that depends on both d(FeC) and d(CN). At the Lu L_3 edge (Figure 7), the three peaks A, B, and C indicate the coordination of the lanthanide atoms with the $\{Fe(CN)_6\}$ building blocks. The first peak, A, represents the single scattering of the first shell (N and O atoms) and depends on d(LuN) and d(LuO). Peak B is a combination between the single scattering of the second shell (C atoms) and the multiple scattering of the Lu–N–C chain. It depends on the parameters d(LuN), d(CN) and $\cos\theta$. Peak B is complicated by the presence of additional DMF molecules around Lu. Lastly, peak C represents the long-range interaction between both cations. It originates from the combined contributions of the single scattering of the third shell (Fe atoms) and the multiple scattering of the Lu–N–C–Fe chain and is influenced by the parameters d(LuN), d(CN), $\cos\theta$, and d(FeC). In the case of **Lu^{III}/Fe^{III}/DMF**, peak C is very weak because only one Fe···Lu interaction occurs per $\{FeCN_6\}$ unit. Therefore, **Lu^{III}/Fe^{III}/DMF** can be considered as a severe test for the parameterized fitting procedure. According to this description, both edges are complementary, because they probe the cyano ligand from the Fe and M (M = lanthanide or actinide) sides. A similar fitting procedure has also been reported in the literature for the compound $Na_2Co[Fe(CN)_6]$.[45] Considering this, both edges of **Lu^{III}/Fe^{III}/DMF** were adjusted together with the series of linked parameters listed above (Figure 7). Instead of eight independent parameters, the remaining floating structural parameters were d(FeC), d(MN), d(CN), and $\cos\theta$. For each coordination shell, the coordination number was fixed: 6C and N around the Fe cation, 8 or 9 (N + water) around the actinide cation. Using this procedure, the distances obtained by the parameterized combined fit and by X-ray diffraction are similar. EXAFS at the Fe K edge: d(FeC) = 1.93(1) Å, σ^2 = 0.0030 $Å^2$, d(FeN) = 3.05(1) Å, σ^2 = 0.0165 $Å^2$, S_0^2 = 0.7, Δe_0 = 5.2 eV, ε = 0.003; EXAFS at the Lu L_3 edge: d(LuO) = 2.28(1) Å, σ^2 = 0.0084 $Å^2$, d(LuN) = 2.40(2) Å, σ^2 = 0.0149 $Å^2$, d(LuC) = 3.48(1) Å, σ^2 = 0.0001 $Å^2$, d(LuFe) = 5.38(2) Å; from the quadruple path σ^2 = 0.0011 $Å^2$, S_0^2 = 1.1, Δe_0 = 7.6 eV, R = 2.5%, and θ = 162(12)°; DRX: (FeC) = 1.94, d(FeN) = 3.08 Å, d(LuO) = 2.32 Å, d(LuN) = 2.37 Å, d(LuC) = 3.48 Å, d(LuFe) = 5.39 Å, and θ = 168°. Although only one Lu–NC–Fe link over 9 Lu neighbors contributes to the signal of interest here, the remarkable agreement between the XRD and EXAFS data validates our fitting procedure. (Again, it must be underlined that the θ value must be considered with care, given the high uncertainty obtained from the fit. This is partly due to the occurrence of only one Lu–NC–Fe bond per cation and also to the closeness of the bond angle to 180°.) As a consequence, the EXAFS spectra at the An L_3 and Fe K edges have all been fitted with this combined two-edge procedure in a manner similar to that described in this section.

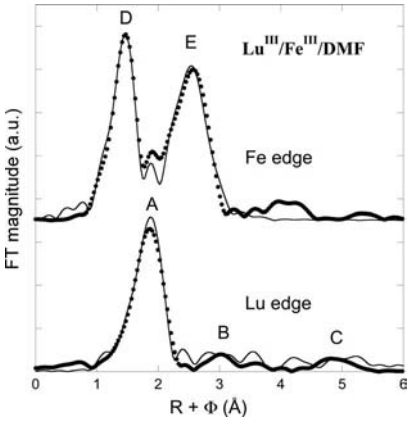

Figure 7. Experimental (solid line) and adjusted (circles) moduli of the Fourier transform of the EXAFS spectrum of **Lu^{III}/Fe^{III}/DMF**. Both Fe K and Lu L_3 edges are presented.

Simulations of the XANES spectra of $KNd^{III}Fe^{II}(CN)_6 \cdot 4H_2O$ (hexagonal *P*63/*m*), $KGd^{III}Fe^{II}(CN)_6 \cdot 3H_2O$ (orthorhombic *Pnma*), and $KGd^{III}Fe^{II}(CN)_6 \cdot 3.5H_2O$ (orthorhombic *Cmcm*) were carried out with the Feff84 code.[44] In the Feff input file, the atomic number of the central atom was changed from that of neodymium to that of americium and gadolinium to californium. All the other structural parameters were kept equal to the crystal structure of the lanthanide compound. XANES calculations were carried out in the SCF mode with FMS calculation with a cluster size of about 7 Å.

Acknowledgments

Support for this research was provided by the CEA, Nuclear Energy Division, Basic Research Program (RBPCH) of the Groupement National de Recherche, PARIS, France and the International Research Staff Exchange Scheme (HEXANE project) of the European Community. XAS measurements were carried out at ESRF/ROBL, a European synchrotron user facility, at SSRL/11-2, a national user facility operated by Stanford University on behalf of the U.S. Department of Energy, Office of Basic Energy Sciences, and at SOLEIL/SAMBA, a French national user facility. The au-

thors would like to thank Valérie Briois, Stéphanie Belin, and Emiliano Fonda (SOLEIL/SAMBA) for their help. They also would like to acknowledge Lester R. Morss for the former loan of ^{249}Cf through the heavy isotopes production program of the U.S. Department of Energy.

[1] C. Cuillerdier, C. Musikas, L. Nigond, *Separation. Sci. Technol.* **1993**, *28*, 155.
[2] D. Li, R. Clérac, O. Roubeau, E. Harté, C. Mathonière, R. Le Bris, S. M. Holmes, *J. Am. Chem. Soc.* **2008**, *130*, 252.
[3] R. K. Hocking, E. C. Wasinger, F. de Groot, K. O. Hodgson, B. Hedman, E. I. Solomon, *J. Am. Chem. Soc.* **2006**, *128*, 10442.
[4] M. Ohba, H. Okawa, *Coord. Chem. Rev.* **2000**, *198*, 313.
[5] H. Svendsen, O. Overgaard, M. Chevallier, E. Collet, P. B. Iversen, *Angew. Chem.* **2009**, *121*, 2818; *Angew. Chem. Int. Ed.* **2009**, *48*, 2780.
[6] Y. Kulyako, P. Moisy, M. Lecomte, C. Madic, T. Tofimov, S. Perevalov, M. Samsonov, B. Myasoedov, *Radiochim. Acta* **2003**, *91*, 5.
[7] G. W. Beall, D. F. Mullica, W. O. Milligan, *Acta Crystallogr., Sect. B* **1978**, *34*, 1446.
[8] D. F. Mullica, W. O. Milligan, J. D. Oliver, *Inorg. Nucl. Chem. Lett.* **1979**, *15*, 1.
[9] D. F. Mullica, E. L. Sappenfield, H. O. Perkins, *J. Solid State Chem.* **1988**, *73*, 65.
[10] W. O. Milligan, D. F. Mullica, H. O. Perkins, *Inorg. Chim. Acta* **1982**, *60*, 35.
[11] D. F. Mullica, E. L. Sappenfield, *Powder Diffr.* **1989**, *4*, 101.
[12] D. F. Mullica, E. L. Sappenfield, H. O. Perkins, *J. Solid State Chem.* **1989**, *78*, 301.
[13] F. Goubard, A. Tabuteau, *J. Solid State Chem.* **2002**, *167*, 34.
[14] F. Goubard, A. Tabuteau, *Struct. Chem.* **2003**, *14*, 257.
[15] D. F. Mullica, E. L. Sappenfield, T. A. Cunningham, *J. Solid State Chem.* **1991**, *91*, 98.
[16] X. L. Xu, F. Hulliger, *Eur. J. Solid State Inorg. Chem.* **1990**, *27*, 443.
[17] D. F. Mullica, J. L. Ward, E. L. Sappenfield, *Acta Crystallogr., Sect. C* **1996**, *52*, 2952.
[18] F. Hulliger, M. Landolt, H. Vetsch, *J. Solid State Chem.* **1976**, *18*, 283.
[19] W. Xiaoyu, Y. Yukawa, Y. Masuda, *J. Alloys Compd.* **1999**, *290*, 85.
[20] L. P. Zhang, X. J. Zhou, T. C. Mak, P. A. Tanner, *Polyhedron* **2007**, *26*, 4019.
[21] A. Domman, H. Vetsch, F. Hulliger, *Acta Crystallogr., Sect. C* **1990**, *46*, 1992.
[22] M. C. Navarro, E. V. Pannunzio-Miner, S. Pagola, M. I. Gomez, R. E. Carbonio, *J. Solid State Chem.* **2005**, *178*, 847.
[23] X. Zhou, W.-T. Wong, M. D. Faucher, P. A. Tanner, *J. Solid State Chem.* **2008**, *181*, 3057.
[24] G. T. Seaborg, J. J. Katz, *The Actinide Elements*, Mc Graw-Hill Book Company, Inc., New York, Toronto, London, **1954**, vol. 14B, p. 427.
[25] J. Krtil, *Radiochim. Acta* **1967**, *7*, 30.
[26] L. P. Zhang, P. A. Tanner, T. C. Mak, *Eur. J. Inorg. Chem.* **2006**, 1543.
[27] X. L. Xu, F. Hulliger, *J. Solid State Chem.* **1989**, *80*, 120.
[28] I. Bonhoure, C. Den Auwer, C. Cartier dit Moulin, P. Moisy, J.-C. Berthet, C. Madic, *Can. J. Chem.* **2000**, *78*, 1305.
[29] N. Tanaka, Y. Kobayashi, M. Kamada, *Bull. Chem. Soc. Jpn.* **1966**, *39*, 2187.
[30] M. J. Willans, R. E. Wasylishen, R. McDonald, *Inorg. Chem.* **2009**, *48*, 4342.
[31] a) R. D. Shannon, *Acta Crystallogr., Sect. A* **1976**, *32*, 751; b) A. Bilewicz, *Radiochim. Acta* **2004**, *92*, 69.
[32] F. David, *J. Less-Common Met.* **1986**, *121*, 27.
[33] P. G. Allen, J. J. Bucher, D. K. Shuh, N. M. Edelstein, T. Reich, *Inorg. Chem.* **1997**, *36*, 4676.
[34] S. Skanthakumar, M. R. Antonio, R. E. Wilson, L. Soderholm, *Inorg. Chem.* **2007**, *46*, 3485.
[35] I. Persson, P. D′Angelo, S. De Panfilis, M. Sandstrom, L. Eriksson, *Chem. Eur. J.* **2008**, *14*, 3056.
[36] P. Lindqvist-Reis, C. Apostolidis, J. Rebizant, A. Morgenstern, R. Klenze, O. Walter, T. Fanghanel, R. G. Haire, *Angew. Chem.* **2007**, *119*, 937; *Angew. Chem. Int. Ed.* **2007**, *46*, 919.
[37] E. Galbis, J. Hernandez-Cobos, C. Den Auwer, C. Le Naour, D. Guillaumont, E. Simoni, R. R. Pappalardo, E. S. Marcos, *Angew. Chem.* **2010**, *122*, 3899; *Angew. Chem. Int. Ed.* **2010**, *49*, 3811.
[38] C. Apostolidis, B. Schimmelpfennig, N. Magnami, P. Lindqvist-Reis, O. Walter, R. Sykora, A. Morgenstern, E. Colineau, R. Caciuffo, R. Klenze, R. G. Haire, J. Rebizant, F. Bruchertseifer, T. Fanghänel, *Angew. Chem.* **2010**, *122*, 6487; *Angew. Chem. Int. Ed.* **2010**, *49*, 6343.
[39] P. D′Angelo, S. De Panfilis, A. Filipponi, I. Persson, *Chem. Eur. J.* **2008**, *14*, 3045.
[40] M. Duvail, P. D′Angelo, M.-P. Gaigeot, P. Vitorge, R. Spezia, *Radiochim. Acta* **2009**, *7*, 339.
[41] D. F. Mullica, J. M. Farmer, B. P. Cunningham, J. A. Kautz, *J. Coord. Chem.* **2000**, *49*, 239.
[42] B. Ravel, M. Newville, *J. Synchrotron Radiat.* **2005**, *12*, 537.
[43] A. Michalowicz, EXAFS code, to be found under http://www.icmpe.cnrs.fr.
[44] J. J. Rehr, R. C. Albers, *Rev. Mod. Phys.* **2000**, *72*, 621.
[45] M. Giorgetti, M. Berrotoni, A. Filipponi, P. Kulesza, R. Marassio, *Chem. Phys. Lett.* **1997**, *275*, 108.

Received: September 20, 2010
Published Online: February 21, 2011

